Microbial Cell Factories

RESEARCH

Open Access

Improving activity of GenB3 and GenB4 in gentamicin dideoxygenation biosynthesis by semi-rational engineering

Hang Zhai[1], Lihua Yang[1], Qi Ye[1], Zhijun Kong[1], Jiye Pei[1], Yuan Ji[1], Botong Liu[1], Xiaotang Chen[1], Tingting Tian[1], Xianpu Ni[1*], Huanzhang Xia[1*] and Shumin Zhang[1*]

Abstract

Background Aminoglycoside antibiotics continue to play an indispensable role in clinical antibacterial agents. However, the protection and deprotection procedures in the chemical pathways of semi-synthetic antibiotics are long, atom- and step-inefficient, which severely hampers the development of novel AGs.

Results Here, GenB3 and GenB4 are employed to synthesize sisomicin, Oxo-verdamicin, Oxo-gentamicin C1a, and Oxo-gentamicin C2a. Subsequently, a semi-rational strategy is applied to enhance the activities of GenB3 and GenB4. The activity of GenB3^{M1} (Q270N) towards JI-20A-P is 1.74 times higher than that of GenB3^{WT}. Similarly, the activity of GenB3^{M2} (L361C/A412T/Q270N) towards JI-20Ba-P is 1.34 times higher than that of GenB3^{WT}. The activity of GenB4^{M1} (L356C) towards sisomicin is 1.51 times higher than that of GenB4^{WT}, while GenB4^{M2} (L356C/A407T/Q265N) towards verdamicin C2a is 1.34 times higher than that of GenB4^{WT}. Furthermore, the beneficial effects of these mutants have been validated in engineered strains. Molecular dynamics simulations indicate that GenB3^{M1} establishes a hydrogen bond network in the active center, while GenB4^{M1} reduces the distance between K238 and the reaction center. It is also noted that the GenB3^{M2} exhibits a synergistic effect specifically on JI-20Ba-P, as the C6′-CH_3 group stabilization restricts the movement of the substrate, which contrasts with JI-20A-P.

Conclusion Our results not only lay the foundation for the mild and efficient synthesis of C6′-modified AGs analogues but also serve as a reference for synthesizing additional single components in *M. echinospora* by further enhancing the dideoxygenation process.

Keywords Gentamicin, Ketone group, Semi-rational engineering, GenB3, GenB4

*Correspondence:
Xianpu Ni
nixianpu126@126.com
Huanzhang Xia
hzxia@syphu.edu.cn
Shumin Zhang
zhangsmo@sohu.com
[1]School of Life Science and Biopharmaceutics, Shenyang Pharmaceutical University, No.103 Wenhua Road, Shenyang, Liaoning, China

Introduction

Since streptomycin can be utilized as a specific treatment for tuberculosis [1], the isolation and identification of aminoglycoside antibiotics (AGs) have entered a golden age. Antibiotics such as kanamycin, tobramycin, gentamicin, and sisomicin have been successively discovered. Subsequently, a series of semi-synthetic AGs have been developed for clinical use to address the serious ototoxic and nephrotoxic side effects as well as drug resistance, such as netilmicin, arbekacin and plazomicin [2], whose primary modification sites are C6'-NH_2 and C1-NH_2 (Scheme 1a). In addition to their antibacterial properties, AGs also exhibit beneficial effects in other areas. For instance, gentamicin can induce apoptosis in tumor cells by activating P53 through the premature termination codon (PTC) effect [3]. Moreover, gentamicin has shown potential in treating ischemic stroke by inhibiting miR-34a [4], while analogues of sisomicin and kanamycin may act as binders for RNA repeat sequences, providing a therapeutic approach for myotonic dystrophy [5, 6]. Furthermore, sisomicin and kanamycin can function as non-ionic, biodegradable delivery vectors to enhance the delivery efficiency of antisense oligonucleotides both in vitro and in vivo [7]. These novel applications underscore the importance of synthesizing AGs with diverse structures. However, selectivity issues in chemical reactions present significant challenges.

Sisomicin was utilized as a precursor for the synthesis of various AGs (Scheme 1b). For example, gentamicin B1 and gentamicin X2 were synthesized through 6 steps yielding between 10% and 14% [8]. Verdamicin C2 (VerC2) and verdamicin C2a (VerC2a) were synthesized through 7 steps, although their yields were below 3% [9]. Additionally, gentamicin C1a (C1a), gentamicin C2b (C2b), gentamicin C2a (C2a), and gentamicin C1 (C1) were synthesized through 6–8 steps with yields ranging from 1.4–12.7% [10, 11]. Xu successfully obtained 24 sisomicin analogues through 8 steps. Among these, AGA-16 demonstrates superior ADME and PK properties [12]. The selective modification in the chemical synthesis of AGs is complicated by the intricate protection and deprotection steps, which contribute to lengthy routes and low yields. Consequently, chemoenzymatic synthesis has garnered significant attention. Ban employed GenN and AAC(6')-APH(2") enzymes to synthesize 3 amikacin analogues [13]. Lee synthesized 4 pseudo-trisaccharide AGs exhibiting enhanced nonsense codon readthrough activity via an acid hydrolysis-KanM2 coupling reaction [14].

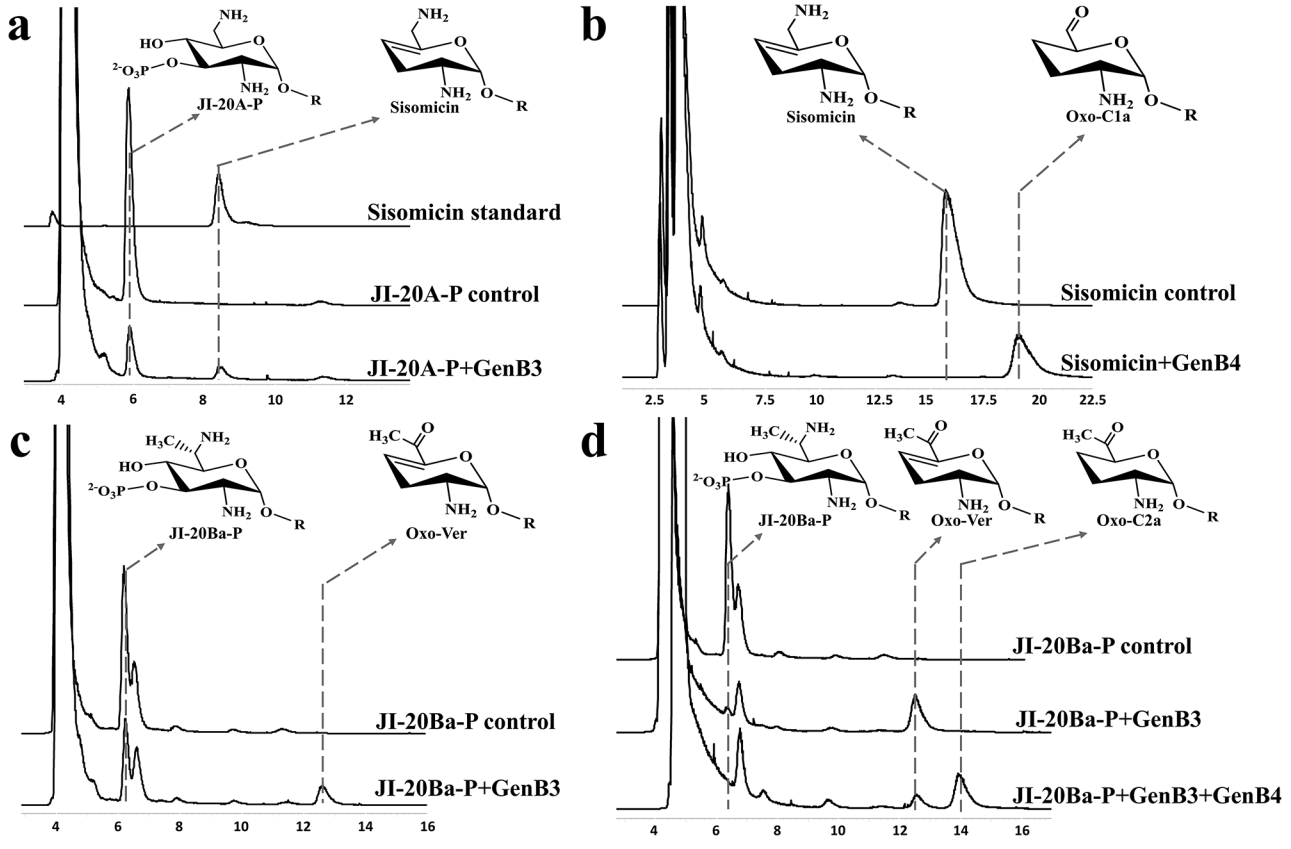

Fig. 1 HPLC-ELSD analysis of the reactions of GenB3 and GenB4. **a**. The catalysis between GenB3 and JI-20A-P; **b**. The catalysis between GenB4 and sisomicin, the mobile phase II was used; **c**. The catalysis between GenB3 and JI-20Ba-P; **d**. GenB4 combined with GenB3 to catalyze JI-20Ba-P. The group of control represents that no enzyme is added

Stojanovski reacted sisomicin with GenB4 to produce Oxo-gentamicin C1a (Oxo-C1a), subsequently yielding 11 novel 6'- C1a analogues by chemically and specifically introducing various groups at the C6' position (Scheme 1c) [15]. The enzymatic introduction of reactive groups such as aldehyde and ketone functionalities, has enabled the synthesis of novel AGs analogues in a green, sustainable, and efficient manner.

Previous studies have shown that dideoxygenation in the gentamicin biosynthesis process involves key precursors for semi-synthetic AGs. GenP phosphorylates JI-20 A and JI-20Ba, after which GenB3 eliminates the phosphate group, resulting in the formation of sisomicin and verdamicin. Subsequently, GenB4 migrates the double bonds to yield C1a and C2a [16–18]. However, research on GenB3 and GenB4 has primarily concentrated on gene function, with a notable lack of studies focusing on protein engineering. Initially, the catalytic characteristics of GenB3 and GenB4 are examined and sisomicin, Oxo-verdamicin (Oxo-Ver), Oxo-gentamicin C1a (Oxo-C1a), and Oxo-gentamicin C2a (Oxo-C2a) are synthesized. Based on the crystal structures of GenB3 (PDB ID: 7LM0) and GenB4 (PDB ID: 7LLD) [17], we employ a semi-rational engineering strategy to enhance the activity of these enzymes. Utilizing *M. echinospora* as the host strain, we construct engineered strains capable of producing single-component sisomicin, Oxo-Ver, C1a, and C2a. The beneficial effects of the GenB3 and GenB4 mutants are validated in these four strains, and the mechanisms underlying the increased activity of the mutants are elucidated through molecular dynamics simulations.

Results and discussion

Lower affinity between C6'-methylated substrates and the enzymes

The dideoxygenation process of gentamicin has been elucidated. In this biological process, sisomicin, VerC2a, C1a, C2a, and C2 are involved. Additionally, keto intermediates such as Oxo-C1a, Oxo-Ver, and Oxo-C2a have been isolated. The characteristics of GenB3 and GenB4 towards different substrates warrant further investigation. To obtain the catalytic substrates of GenB3, JI-20 A, JI-20Ba, and JI-20B were isolated and purified from the fermentation broths of *M. echinospora* ΔKP, *M. echinospora* ΔB2P, *M. echinospora* ΔP. Then, JI-20A-P, JI-20Ba-P, and JI-20B-P were obtained through the catalysis of GenP (Additional file 1: Fig. S1).

When JI-20A-P reacts with GenB3, sisomicin is produced (Fig. 1a), while Oxo-sisomicin is not detected. This absence may be attributed to the GenB3's transamination, with NH_3 or the excess JI-20A-P possibly acting as the amino donor [17]. When sisomicin reacts with GenB4, a complete conversion of 7.5 mM sisomicin to Oxo-C1a occurs (Fig. 1b), aligning with previous findings [15, 16]. When JI-20Ba-P reacts with GenB3, Oxo-Ver is generated (Fig. 1c). In vivo experiments indicate that *M. echinospora* ΔB4 predominantly accumulates Oxo-Ver rather than Verdamicin [16]. After adding GenB4 and an amino donor to the reaction involving JI-20Ba-P and GenB3, Oxo-C2a can be produced (Fig. 1d). However, Oxo-Ver does not directly react with GenB4 to yield Oxo-C2a [16, 18]. Within this coupling system, GenB3 performs a transamination function, converting Oxo-Ver into VerC2a, which is subsequently transformed into the more stable Oxo-C2a by GenB4.

The specific activities of GenB3 in relation to JI-20A-P, JI-20Ba-P, and JI-20B-P were measured at 40.07 U/mg, 9.31 U/mg, and 0.17 U/mg, respectively (Table 1). In parallel, the specific activities of GenB4 towards sisomicin and VerC2a were determined to be 276.11 U/mg and 97.92 U/mg, respectively (Table 3). These findings indicate that both GenB3 and GenB4 exhibit enhanced catalytic efficiencies in the absence of a methyl group at C6' (JI-20 A-P and sisomicin), whereas the presence of a methyl group at C6' results in diminished catalytic efficiencies (JI-20Ba-P, JI-20B-P, and VerC2a). Furthermore, GenB3 demonstrates stereoselectivity and does not recognize the C6'-CH_3(R) substrate. The affinity between the C6'-methylated substrate and GenB3 and GenB4 are low, thereby leading to decreased reaction efficiency.

The identification of key amino acid residues in GenB3

In addition to the influence of the methyl group on the affinity of GenB3 and GenB4, it is important to note that intermediates, such as JI-20A-P and JI-20Ba-P, can be dephosphorylated by phosphohydrolases in vivo, which subsequently impedes the biosynthesis of gentamicin. To mitigate the loss of JI-20A-P and JI-20Ba-P, GenB3 and GenB4 were overexpressed in *M. echinospora*, resulting in a 26.44% increase in the yield of gentamicin (Additional file 1: Fig. S2). This finding suggests that enhancing the levels of GenB3 and GenB4 accelerates the conversion of phosphorylated intermediates, thereby improving the overall yield. Further enhancement of the activities of GenB3 and GenB4 could not only contribute to an increased yield but also hold significant implications for the efficient in vitro synthesis of keto products.

Due to the unsatisfactory docking calculation, a model between GenB3 (PDB ID: 7LM0) with JI-20Ba-P was built by superimposition and deletion. The residues in the pocket were similar to the binding pocket reported by Li [17] for GenB3 with JI-20Ba-P. The binding pocket is primarily divided into three regions: the PLP binding region, the catalytic region, and the backbone stabilization region (Fig. 2a). In the PLP binding region, T114, G115, S116, and G271 form hydrogen bonds with the phosphate groups of PLP, while V218 interacts with pyridine ring through σ-π interactions. When the substrate

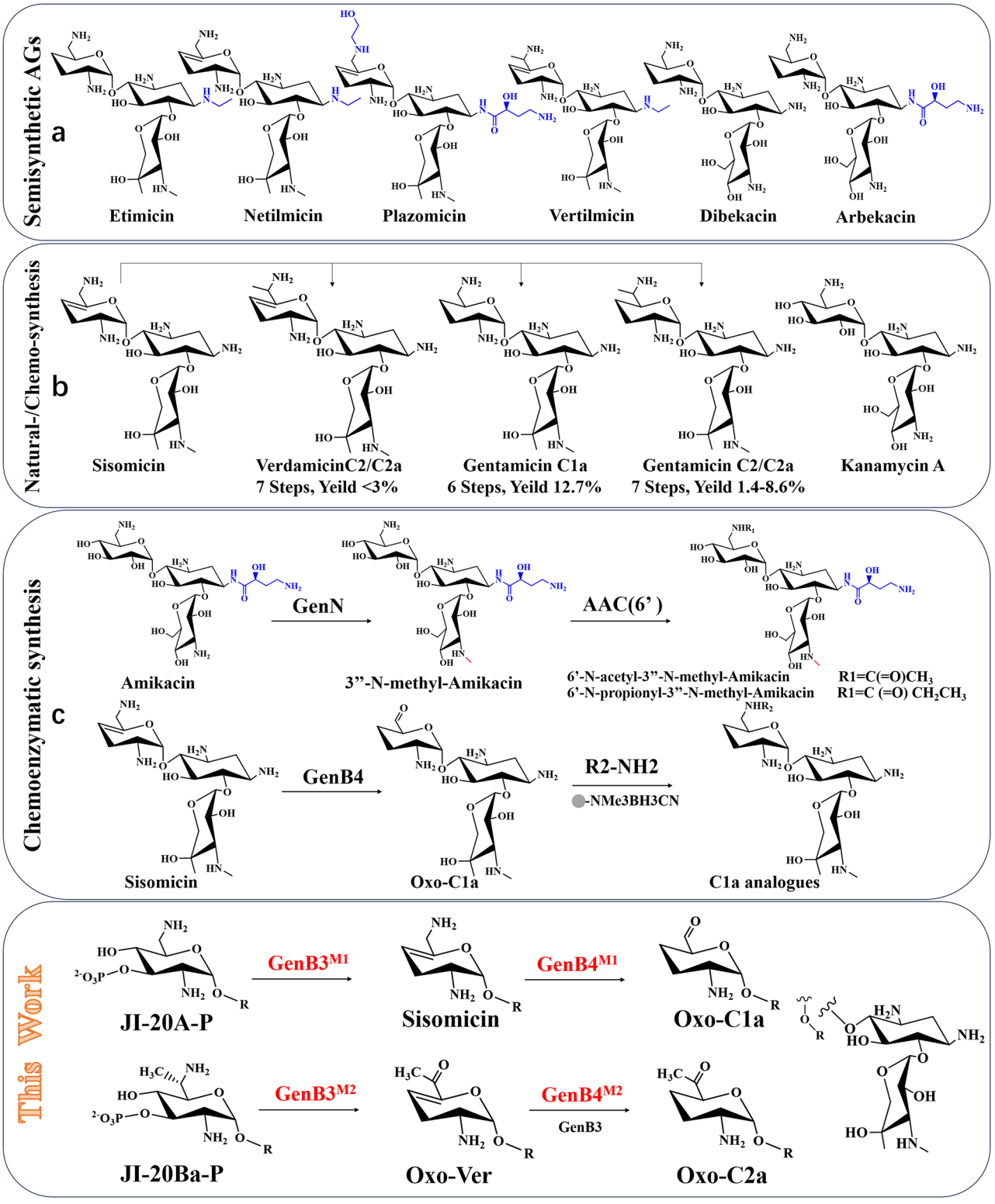

Scheme 1 The enzymatic synthesis of easily reactive products using GenB3 and GenB4

Table 1 The specific activity of GenB3^{WT} and its mutants (U/mg)[a]

	JI-20A-P	JI-20Ba-P	JI-20B-P
GenB3^{WT}	40.07 ± 4.58	9.31 ± 1.12	0.17 ± 0.09
GenB3^{Q270N}	44.11 ± 4.22	14.64 ± 0.69	1.30 ± 0.16
GenB3^{L361C}	30.64 ± 1.83	13.50 ± 1.61	-
GenB3$^{T359C/Q270N}$	28.23 ± 1.82	12.21 ± 0.50	-
GenB3$^{L361C/Q270N}$	30.55 ± 3.64	14.45 ± 0.53	-
GenB3$^{L361C/A412T/Q270N}$	20.75 ± 3.95	17.63 ± 0.85	-

[a]The reaction system consists of: substrate 2 mmol/L, PLP 0.75 mmol/L, HEPES (50 mmol/L, pH 7.0), GenB3 25 μmol/L. The JI-20A-P reacts for 2 h, the JI-20Ba-P reacts for 4 h, and the JI-20B-P reacts for 12 h at 30 °C. Following the reaction, chloroform is used to stop the reaction, and after filtration, HPLC-ELSD analysis is performed. The substrate consumption is calculated based on the peak area, and 1 unit of enzymatic activity is defined as the amount of enzyme required to consume 1 μmol/L of substrate per minute. (-) no substrate was consumed

enters, it forms an external aldimine, which is accompanied by the dissociation of K243, and T272 may stabilize K243. In the catalytic region, the C3' phosphate group is accommodated by Y24, S57, E355, S357, Q270 and R275 (Fig. 2b). Q270 not only resides on the channel in which the substrate enters the pocket but also forms a hydrogen bond with the C4'-OH. In the backbone stabilization region, D331 forms a hydrogen bond with N3" on ring III, while A412 establishes a hydrogen bond with N1. The residues Y219, E190, L191, L192, F413, and F408 shape the pockets that accommodate rings III and I, anchoring the substrate within these pockets.

To obtain beneficial mutants, we mutated the residues to smaller amino acids. For example, Q270 was mutated to D, N, T, S, A, or G; Y219 was mutated to S, N, D, or T; R275 was mutated to A or G; and F413 was mutated to S, T, or M. We also selected the basic amino acids in the catalytic region to provide stronger interactions with the phosphate group, such as Y24K and E355R. Based on the amino acid conservation (Fig. 2c), we mutated the amino acids in the pocket to more conserved ones, such as Y24W, L191P, Y219I, and S357G. In the alanine scan of eight residues in the pocket, T359C and L361C were identified as enhancing the catalytic activity for JI-20Ba-P [19]. Based on conservation analysis, the mutations Q360H and L361M were proposed.

Site-directed mutagenesis of key amino acids in GenB3

To construct the mutants using the overlap extension PCR method, the initial screening was performed using a crude enzyme reaction. In the reaction with JI-20A-P, many mutants showed lower relative activity compared to the GenB3^{WT}. However, we found that the relative activity of the GenB3^{Q270N} was 2.5 times higher than that of GenB3^{WT}. Additionally, GenB3^{M329C}, GenB3^{F413M}, and GenB3^{A412T} displayed slight improvements (Fig. 3a). For JI-20Ba-P, GenB3^{L361C} and GenB3^{T359C} exhibited the most notable increases in activity, with relative activities of 3.5 times and 3.0 times higher than that of GenB3^{WT}, respectively. We also observed enhancements in the relative activity of GenB3^{Q270N}, GenB3^{Q270S}, GenB3^{M329C}, GenB3^{A412T}, and GenB3^{F413M}. Furthermore, GenB3^{E190S}, GenB3^{S242A}, and GenB3^{F413A} showed minor improvements (Fig. 3b). However, none of the mutant demonstrated improved activity for JI-20B-P, indicating that these mutants did not alter the stereoselectivity (Additional file 1: Fig. S3).

Promotion of GenB3's activity through combinatorial mutagenesis

To avoid getting trapped in local minima, mutations that significantly enhance activity, as well as those that provide moderate improvements, were selected for combined mutations. The GenB3^{L361C}, GenB3^{T359C}, and GenB3^{M329C} exhibited enhanced activity, and all are located near Y219, indicating that these positions may serve similar functions. Based on the findings from L361C, T359C, and M329C, combinations with the mutations S242A, Q270N, Q270S, A412T, and F413M were investigated.

In the case of JI-20A-P, many mutants exhibited comparable activity to that of GenB3^{WT}, with no mutant demonstrating higher activity than GenB3^{Q270N}. Conversely, many mutants displayed increased activity for JI-20Ba-P, their levels were comparable to those of GenB3^{L361C} and GenB3^{T359C}. Notably, only the combinations GenB3$^{L361C/Q270N}$ and GenB3$^{T359C/Q270S}$ exhibited a significant increase in activity compared to GenB3^{L361C} (Fig. 4). Furthermore, when L361C, T359C, and M329C were combined with A412T or F413M, the mutants showed reduced activity for both substrates, suggesting a potential negative interaction between these residues and A412T or F413M.

L361C, T359C, Q270N, and A412T were selected for combination. Fortunately, the GenB3$^{L361C/A412T/Q270N}$ showed a significant increase towards JI-20Ba-P, establishing it as the optimal mutant among all tested mutants (Fig. 4). However, this combination showed a decreased activity for JI-20A-P. Subsequently, GenB3^{Q270N}, GenB3^{L361C}, GenB3$^{Q270N/T359C}$, GenB3$^{Q270N/L361C}$, and GenB3$^{Q270N/L361C/A412T}$ were chosen for the specific enzymatic assay (Additional file 1: Fig. S4). For JI-20A-P, the enzyme activity of GenB3^{WT} was measured at 40.07 U/mg, whereas GenB3^{Q270N} exhibited higher activity at 44.11 U/mg. For JI-20Ba-P, the enzyme activity of GenB3^{WT} was measured at 9.31 U/mg, whereas GenB3^{Q270N} exhibited higher activity at 14.64 U/mg. The activity of the GenB3$^{L361C/A412T/Q270N}$ further increased to 17.63 U/mg (Table 1), indicating a synergistic effect among L361C, A412T, and Q270N for JI-20Ba-P.

Kinetic parameters of GenB3 and its mutants

The kinetic parameters for GenB3^{WT}, GenB3^{Q270N}, and GenB3$^{L361C/A412T/Q270N}$ were determined for both

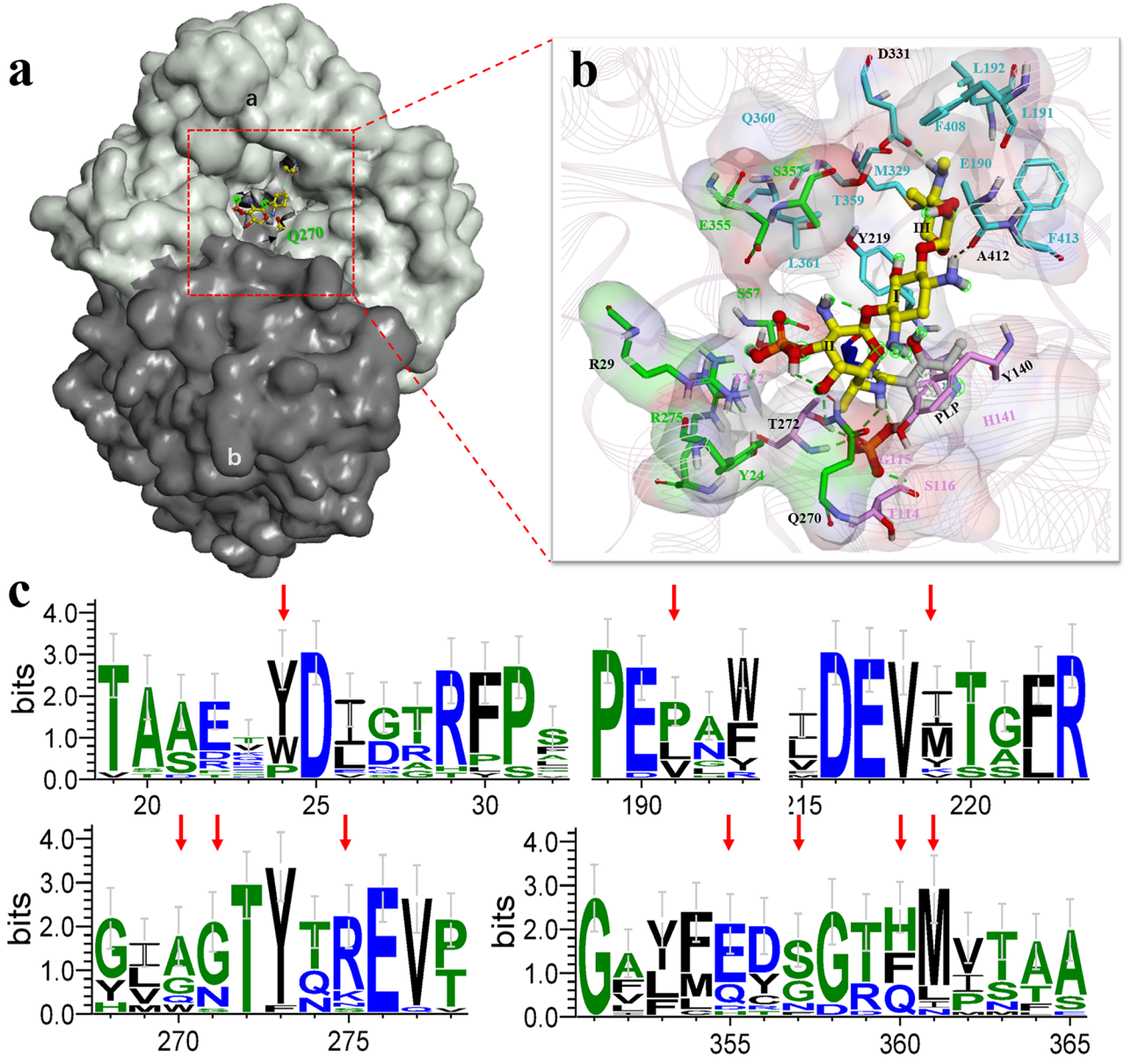

Fig. 2 The binding pocket and amino acid conservation of GenB3. **a**. The spatial conformation of GenB3 (PDB ID:7LM0) in complex with JI-20Ba-P; **b**. Analysis of key residues in the binding pocket of JI-20Ba-P-PLP. The yellow stick model represents JI-20Ba-P, the gray stick model represents PLP, green amino acids indicate the substrate catalytic region, purple-pink amino acids denote the PLP binding region, blue amino acids represent the substrate scaffold stabilizing the binding region, and black font amino acids are involved in hydrogen bonding with the substrate; **c**. Analysis of the conservation of amino acids in the binding pocket, with red arrows indicating positions mutated to other amino acids

JI-20A-P and JI-20Ba-P. The parameters were assessed by detecting the release of phosphate ions using the molybdate blue detection method [20], which allowed for the determination of initial reaction velocities. Nonlinear fitting was employed to calculate the *Km* and *Kcat* values (Additional file 1: Fig. S5).

For JI-20A-P, the *Km* and *Kcat* for GenB3^{WT} were 0.50 mM and 1.78 min^{-1}, respectively. GenB3^{Q270N} exhibited the lowest *Km* value of 0.25 mM, resulting in an increase in the *Kcat/Km* value from 3.56 $min^{-1}{\cdot}mM^{-1}$ to 6.20 $min^{-1}{\cdot}mM^{-1}$, which is 1.74 times higher than that of GenB3^{WT} (Table 2). In the case of GenB3$^{L361C/A412T/Q270N}$, the *Kcat/Km* was 2.73 $min^{-1}{\cdot}mM^{-1}$, potentially accounting for the observed decrease in activity. For JI-20Ba-P, GenB3^{Q270N} demonstrated an increased *Kcat/Km* value from 2.34 $min^{-1}{\cdot}mM^{-1}$ to 2.88 $min^{-1}{\cdot}mM^{-1}$ (Table 2). GenB3$^{L361C/A412T/Q270N}$ showed the lowest *Km* value of 1.52 mM, with a *Kcat/Km* value of 3.13 $min^{-1}{\cdot}mM^{-1}$, which was 1.34 times higher than that of GenB3^{WT},

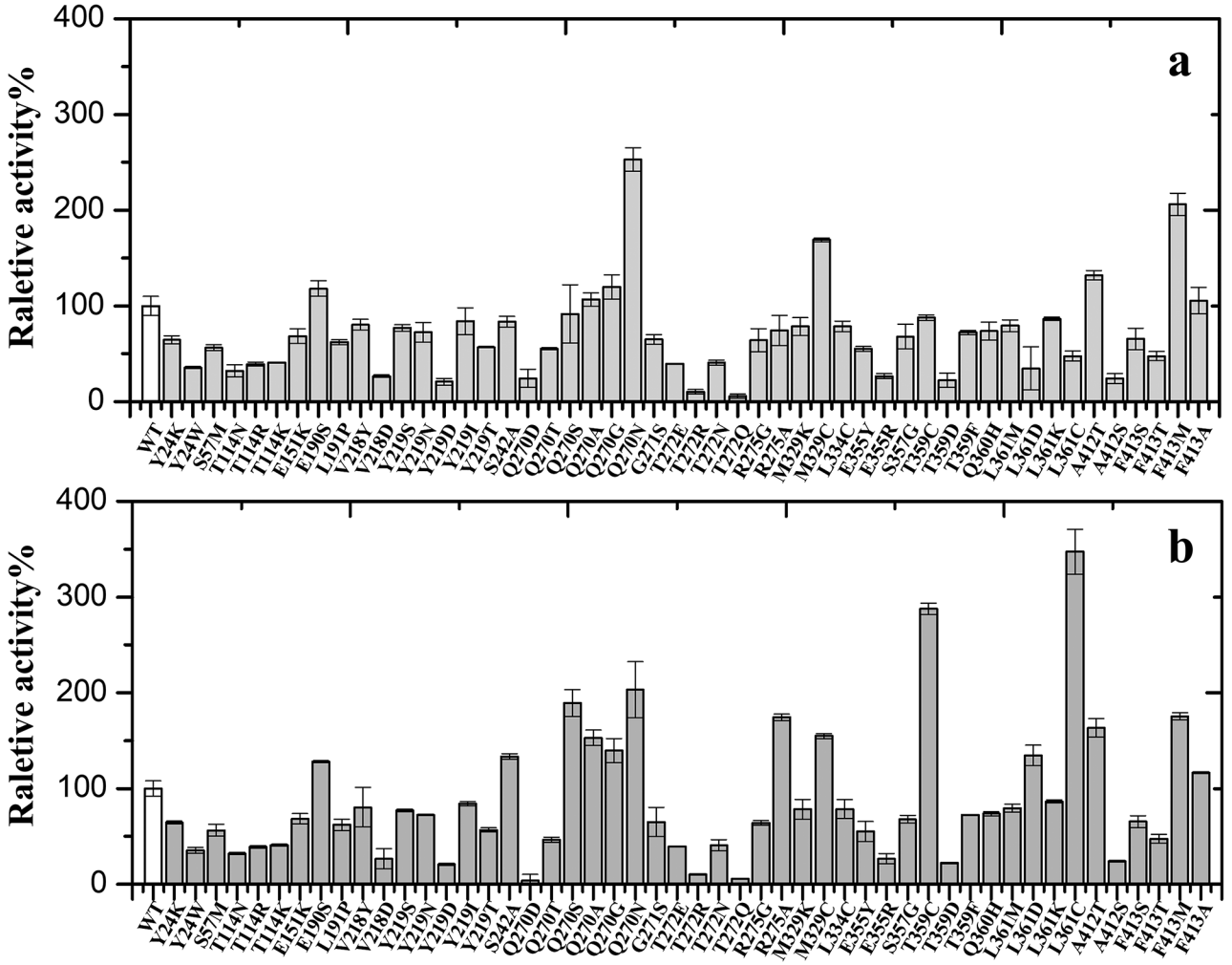

Fig. 3 Dideoxygenation of two phosphorylated substrates by GenB3^{WT} and its mutants. **a**. substrates used were JI-20A-P; **b**. substrates used were JI-20Ba-P. The white-filled bars represent the GenB3^{WT}, while the light gray-filled bars represent the single-point GenB3 mutants. The crude enzymatic reaction contains 2 mM phosphorylated substrate, 0.75 mM PLP, and GenB3 crude solution, which is obtained from the supernatant of disrupted cells with a wet weight concentration of 100 g/L

indicating that there is good synergistic action between Q270N, L361C, and A412T.

Beneficial mutants of GenB4 obtained by parallel amino acid

The amino acid sequences of GenB4 and GenB3 share 83.78% identity, and their crystal structures exhibit high similarity with an RMSD value of 0.47 Å. Given the substantial structural similarity between the two enzymes, it raises the question of whether the beneficial mutants identified in GenB3 might also confer positive effects in GenB4. To explore this possibility, the mutations Q270N, L361C, and A412T from GenB3 were introduced at the parallel positions in GenB4 (Q265N, L356C, and A407T).

The reactions involving GenB4 and seven mutants were conducted with sisomicin. Following the optimization of the reaction system, GenB4 successfully converted sisomicin into Oxo-C1a and a minor quantity of C1a, while a substantial amount of substrate remained unreacted. In contrast, the reaction using GenB4^{L356C} yielded higher amounts of both Oxo-C1a and C1a (Additional file 1: Fig. S6a). The specific activity of GenB4^{L356C} was measured at 418.28 U/mg, which was 1.51 times higher than that of GenB4^{WT} (Table 3). These findings suggest that under identical conditions, GenB4^{L356C} enhances the conversion of sisomicin. We evaluated the activity of GenB4 through the combined catalysis of GenB3 and GenB4 on JI-20Ba-P. If the activity of GenB4 is enhanced, the accumulation of Oxo-Ver will be reduced. The results indicated that the level of Oxo-Ver in GenB4$^{L356C/A407T/Q265N}$ was lower than that in the GenB4^{WT} (Additional file 1: Fig. S6b). The specific activity of GenB4^{WT} was measured at 97.92 U/mg. The enzyme activities of GenB4^{Q265N}, GenB4^{L356C},

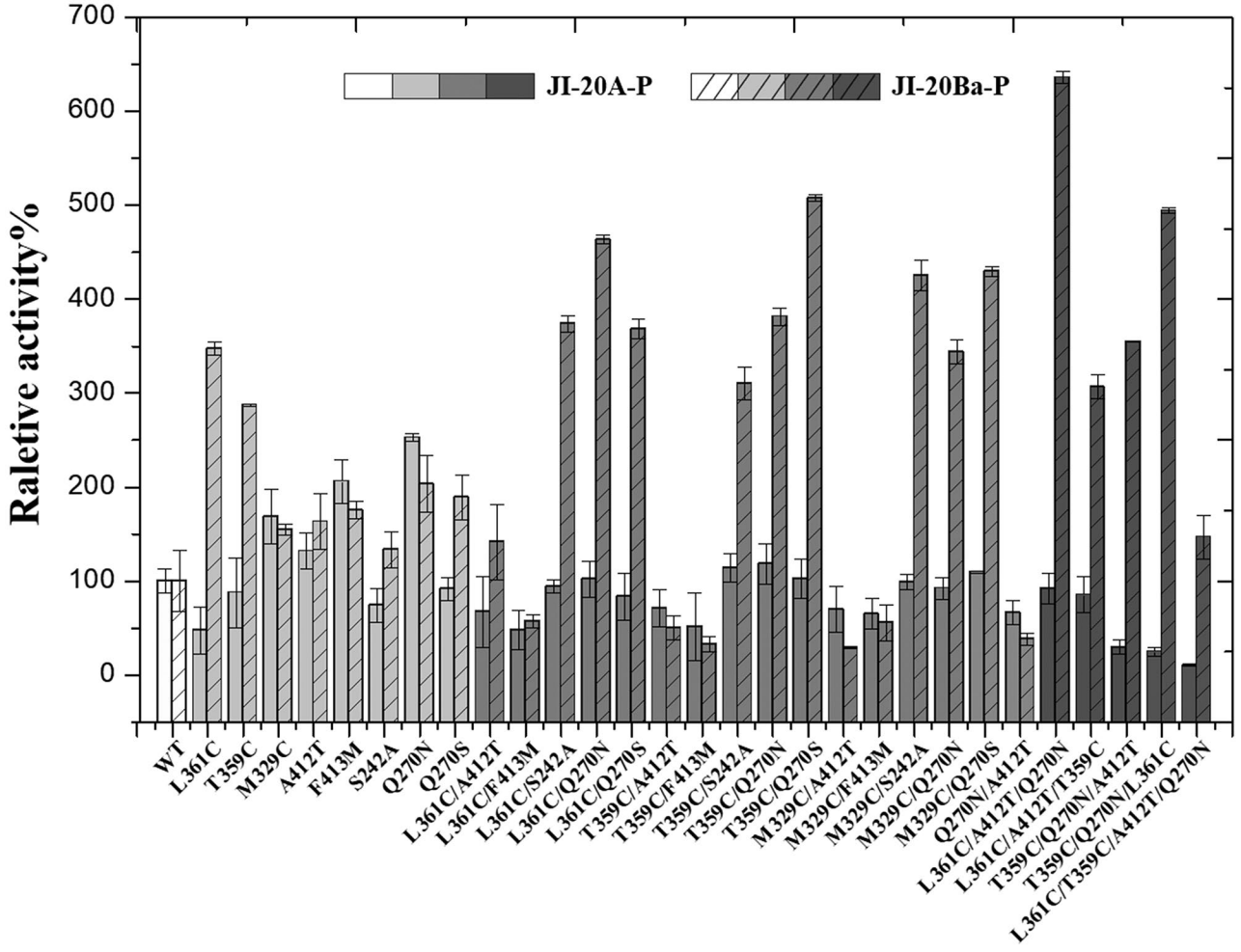

Fig. 4 Dideoxygenation of two phosphorylated substrates by combinatorial GenB3 mutants. The white-filled bar represents the GenB3^{WT}, the light gray-filled bar represents the single-point mutant, the gray-filled bar represents the double-point mutant, and the dark gray-filled bar represents the triple and quadruple mutants. Among these bars, those without a black hatched background correspond to the JI-20A-P, while those with a black hatched background correspond to the JI-20Ba-P

Table 2 Kinetic parameters of GenB3^{WT} and its mutants [a]

Substrate	Entry Enzyme	K_m (mmol/L)	K_{cat} (/min)	K_{cat}/ K_m (L/mmol·min)	Fold
JI-20 A-P	GenB3^{WT}	0.50 ± 0.04	1.78 ± 0.02	3.56	
	GenB3^{Q270N}	0.25 ± 0.02	1.55 ± 0.04	6.20	1.74
	GenB3$^{L361C/A412T/Q270N}$	0.44 ± 0.04	1.20 ± 0.17	2.73	0.77
JI-20Ba-P	GenB3^{WT}	2.81 ± 0.19	6.57 ± 0.45	2.34	
	GenB3^{Q270N}	1.63 ± 0.02	4.70 ± 0.20	2.88	1.23
	GenB3$^{L361C/A412T/Q270N}$	1.52 ± 0.07	4.75 ± 0.21	3.13	1.34

[a]The enzyme reaction system as follows: JI-20A-P and JI-20Ba-P at 100–1900 μmol/L, α-KG 50 μmol/L, PLP 0.75 mmol/L, and HEPES buffer 50 mmol/L. The reaction mixture is preheated at 30 °C. GenB3 or its mutant is added at 10 μmol/L, and after 15 min, 25 μL of the reaction solution is transferred to a 96-well plate containing 75 μL of color development solution. The mixture is allowed to react at room temperature for 5 min, after which 75 μL of termination solution is added. The absorbance at 655 nm is measured, and the results are incorporated into a standard curve prepared with K_2HPO_4 to calculate the released phosphate and reaction rate

GenB4^{A407T}, GenB4$^{L356C/A407T}$, GenB4$^{L356C/Q265N}$ and GenB4$^{A407T/Q265N}$ were all slightly elevated (Table 3). Notably, GenB4$^{L356C/A407T/Q265N}$ exhibited the highest activity, reaching 130.43 U/mg, which is 1.33 times higher than that of GenB4^{WT}.

Beneficial mutants accelerated the biotransformation in the engineered strains

Sisomicin serves as the precursor of plazomicin and etimicin, while C1a is the precursor of netilmicin. Oxo-Ver and Oxo-C2a, which possess a keto group at C6', can be

Table 3 The specific activity of GenB4^{WT} and its mutants (U/mg)

	Sisomicin[a]	VerC2a[b]
GenB4^{WT}	276.11 ± 19.17	97.92 ± 16.88
GenB4^{Q265N}	220.90 ± 21.16	99.13 ± 12.08
GenB4^{L356C}	418.28 ± 6.21	121.13 ± 22.55
GenB4^{A407T}	306.33 ± 28.98	113.99 ± 18.41
GenB4$^{L356C/A407T}$	236.82 ± 19.00	107.97 ± 13.34
GenB4$^{L356C/Q265N}$	357.16 ± 30.96	115.49 ± 14.52
GenB4$^{A407T/Q265N}$	184.61 ± 16.90	112.43 ± 11.45
GenB4$^{L356C/A407T/Q265N}$	218.63 ± 20.93	130.43 ± 13.80

(a) The reaction system of sisomicin: sisomicin 12 mmol/L, PLP 0.75 mmol/L, HEPES (50 mmol/L, pH 7.0), GenB4 at 7.5 μmol/L. After reacting at 30 °C for 2 h, the reaction is terminated with chloroform, followed by membrane filtration and HPLC-ELSD analysis. The amount of product generated is calculated based on the peak area. (b) The reaction system of Oxo-Ver: JI-20Ba-P at 2 mmol/L, PLP at 0.75 mmol/L, Glu at 5 mmol/L, HEPES (50 mmol/L, pH 7.0), GenB3 at 25 μmol/L. After reacting at 30 °C for 12 h, the substrate is completely converted to Oxo-Ver. GenB4 and its mutants at 15 μmol/L are added, and the reaction continues for 2 h before terminating with chloroform. After membrane filtration, HPLC-ELSD analysis is conducted, and the consumption of Oxo-Ver is calculated based on the peak area. 1 U of enzyme activity is defined as the amount of enzyme required to consume 1 μmol/L of substrate per minute

directly chemically modified to obtain analogues. The engineering strains with a single component for the de novo synthesis of these compounds are of great significance for the semi-synthesis of AGs. *M. echinospora* ΔKB4 mainly produces sisomicin and G-52 impurity. By knocking out *gen*L from this strain, *M. echinospora* ΔKB4L was obtained, which solely produces sisomicin with a chemical titer of 194 ± 23 μg/mL. *M. echinospora* ΔK predominantly produces C1a and C2b. Knocking out *gen*L from this strain resulted in *M. echinospora* ΔKL, which solely produces C1a with a chemical titer of 239 ± 36 μg/mL. *M. echinospora* ΔB4 mainly produces Oxo-Ver with a chemical titer of 183 ± 28 μg/mL. A double-knockout strain *M. echinospora* ΔB2L was constructed, leading to the accumulation of Oxo-C2a and C2a. After self-isomerization of Oxo-C2a, ZL101 was generated [21]. The total yield of the two is 229 ± 18 μg/mL (Additional file 1: Fig. S7, Fig. S8a).

Four mutants individually enhanced the activity towards four natural substrates. GenB3^{Q270N} promoted the transformation of JI-20A-P to sisomicin, while GenB3$^{L361C/A412T/Q270N}$ facilitated the conversion of JI-20Ba-P to Oxo-Ver. These mutants were named as GenB3^{M1} and GenB3^{M2}, respectively. GenB4^{L356C} enhanced the transformation of sisomicin to C1a, and GenB4$^{L356C/A407T/Q265N}$ enhanced the transformation of VerC2a to Oxo-C2a, which were named as GenB4^{M1} and GenB4^{M2}, respectively. To investigate whether these mutants would also exhibit beneficial effects in vivo, suitable promoters were selected for overexpression in the engineered strains that synthesize sisomicin, C1a, Oxo-Ver, and Oxo-C2a (Additional file 1: Fig. S8b). After overexpressing GenB3^{M1} using the *SRL37* promoter in *M. echinospora* ΔKB4L, the yield of sisomicin reached 298 ± 8 μg/mL, representing a 39.91% increase compared to the overexpression of GenB3^{WT}. This indicates that GenB3^{M1} can convert JI-20A-P to more sisomicin in vivo. Similarly, after overexpressing GenB4^{M1} using the *kas*Op* promoter in *M. echinospora* ΔKL, the yield of C1a reached 346 ± 17 μg/mL, which was an increase of 26.74% compared to GenB4^{WT} (Fig. 5). This suggests that GenB4^{M1} can facilitate the conversion of sisomicin to a higher quantity of C1a in vivo.

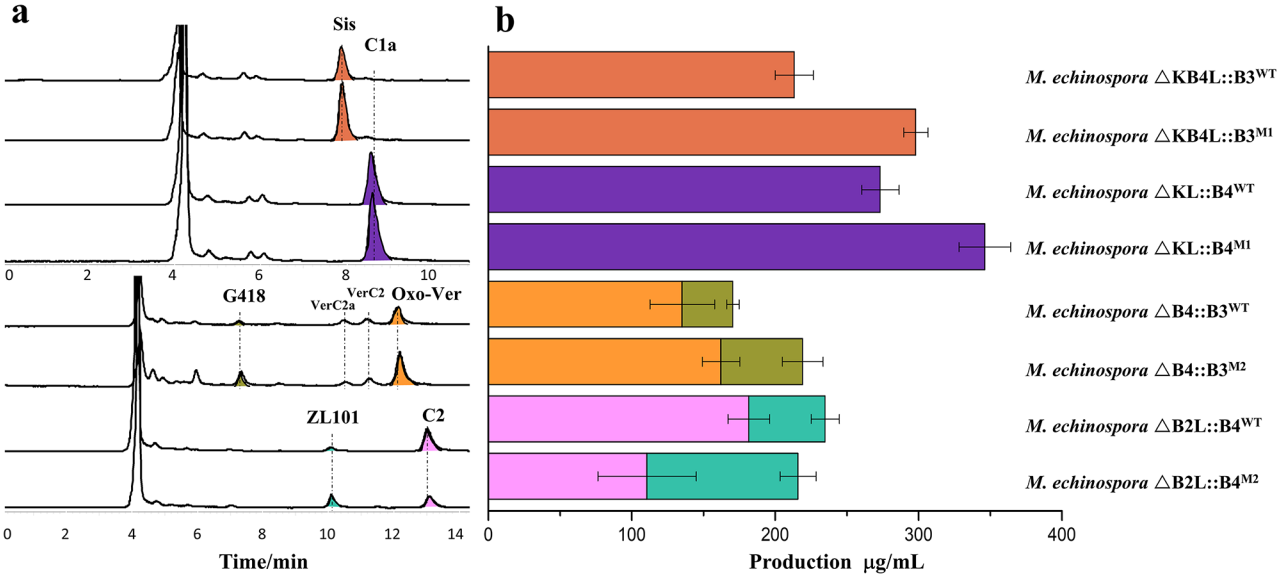

Fig. 5 The overexpression of GenB3 and GenB4 mutants in engineered strains. **a**. HPLC-ELSD analysis of overexpressing four mutants in engineered strains. **b**. Production of overexpressing four mutants in engineered strains. The GenB3 mutants were overexpressed in *M. echinospora* ΔKB4L and *M. echinospora* ΔB4, while the GenB4 mutants were overexpressed in *M. echinospora* ΔKL and *M. echinospora* ΔB2L

In *M. echinospora* ΔB4, the overexpression of GenB3^{M2} using the *SRL37* promoter resulted in a 20.01% increase in the yield of Oxo-Ver compared to GenB3^{WT}. Although the yields of VerC2 and VerC2a exhibited slight increases, the accumulation of G418 also rose, leading to an overall metabolic flux increase of 21.18%. This finding indicates that GenB3^{M2} effectively converts JI-20Ba-P into a greater quantity of Oxo-Ver and enhances metabolic flux. In *M. echinospora* ΔB2L, the overexpression of GenB4^{M2} utilizing the *kas*Op * promoter led to a remarkable 97.36% increase in the yield of ZL101. However, the yield of C2a decreased, and there was no overall increase in metabolic flux. This suggests that GenB4^{M2} preferentially promotes the production of more Oxo-C2a but does not facilitate the synthesis of C2a, which aligns with the results obtained from in vitro experiments.

Molecular dynamic simulation in the pre-reaction state

To further understand the impact of mutations on the structure and activity of GenB3 (PDB ID:7LM0) and GenB4 (PDB ID:7LLD), molecular dynamics (MD) simulations were conducted for 100 ns on the complexes formed between the wild-type proteins (GenB3^{WT} and GenB4^{WT}) and their representative mutants (GenB3^{M1}, GenB3^{M2}, GenB3^{M3}, and GenB4^{M1}) with their respective substrates. These simulations aimed to replicate structural changes under realistic environmental conditions. Here, GenB3^{M3} corresponds to GenB3^{Q270D} and serves as a negative control for the JI-20A-P group.

The RMSD and RMSF during the MD simulation were presented in Additional file 1: Fig. S9, indicating that all systems reached a stable state. Subsequently, the binding free energy was calculated using MM/GBSA (Table 4) to investigate the strength of the interaction between the enzyme and the substrate. The results revealed that the total binding free energy of GenB3^{M1} and GenB3^{WT} with JI-20A-P was nearly identical (-222.44 kcal/mol and – 223.39 kcal/mol, respectively), and these two mutants exhibited the most negative binding energies compared to the others. This finding suggests that GenB3^{M1} and GenB3^{WT} possess a stronger binding affinity for JI-20A-P, aligning with the experimental results. In contrast, the binding free energies for GenB3^{M2} and GenB3^{M3} with JI-20A-P were – 181.21 kcal/mol and – 156.39 kcal/mol, respectively, indicating a significant reduction in their binding capabilities compared to GenB3^{WT}. This reduction likely leads to decreased stability of the substrate within the active site. Through MM/GBSA analysis of residue energy contributions, it was observed that residues R29, T114, G115, K243, T272, and R275 significantly contribute to the binding energy across all systems, highlighting their crucial role in substrate binding. Notably, both GenB3^{M2} and GenB3^{M3} exhibit significantly lower energy contributions at the K243 and R275 positions compared to GenB3^{M1} and GenB3^{WT} (Additional file 1: Fig. S10). This discrepancy is likely an intrinsic factor contributing to the substantial decrease in catalytic activity observed in GenB3^{M2} and GenB3^{M3}.

To investigate the molecular mechanisms underlying the altered efficiency of GenB3^{M1} and GenB3^{M2}, we analyzed the conformations of GenB3^{WT} and its mutants in complex with JI-20A-P. The Q270 forms hydrogen bonds exclusively with the C4'-OH (Fig. 6a). Interestingly, the NH_2 in N270 not only forms hydrogen bonds with the C4'-OH but also the ketone group interacts with Y24 and R275 (Fig. 6b), thereby creating a tight hydrogen bond network among the catalytic residues Y24, R29, R275, and N270. This network stabilizes catalytic residues R29 and R275, facilitating the departure of the C3'-PO_3 and C4'-OH. However, when Q270 is mutated to D, no hydrogen bonds are formed at position 270 (Fig. 6d). This diminished interaction strength is the primary reason for the decreased activity observed in GenB3^{M3}. Upon overlaying GenB3^{WT} and GenB3^{M2}, we noted that JI-20A-P undergoes significant movement (Additional file 1: Fig. S11a). The substrates in rings I and III are positioned deeper within the binding pocket of GenB3^{M2}, resulting in an increased distance between C3'-PO_3 and residues

Table 4 MM/GBSA binding free energy of all complexes

Substrate	Protein	ΔE_{VDW}	ΔE_{EL}	ΔE_{GB}	ΔE_{SURF}	ΔE_{Total}
JI-20A-P	GenB3^{WT}	-136.56	1014.35	-1079.11	-22.07	-223.39
	GenB3^{M1}	-128.94	1029.21	-1101.03	-21.70	-222.44
	GenB3^{M2}	-135.48	1106.85	-1131.01	-21.57	-181.21
	GenB3^{M3}	-136.02	1502.01	-1500.95	-21.42	-156.39
JI-20Ba-P	GenB3^{WT}	-129.85	998.31	-1046.10	-21.20	-198.85
	GenB3^{M1}	-132.54	1116.89	-1140.78	-20.65	-177.08
	GenB3^{M2}	-123.88	932.20	-1013.55	-21.01	-226.24
Sisomicin	GenB4^{WT}	-117.74	47.43	-76.88	-16.75	-163.94
	GenB4^{M1}	-124.46	75.35	-104.64	-17.56	-171.31

Note: The unit of binding free energy is kcal/mol; ΔE_{VDW} and ΔE_{EL} represent the van der Waals interaction energy and electrostatic interaction energy between molecules, which are an important part of the non-covalent interaction between the enzyme and the substrate; ΔE_{GB} and ΔE_{SURF} respectively represent polar solvation energy and nonpolar solvation energy, which is an energy term describing the solvation effect around the enzyme; ΔE_{Total} represents the total binding free energy between the enzyme and the substrate in the system, indicating the binding between the enzyme and the substrate strength

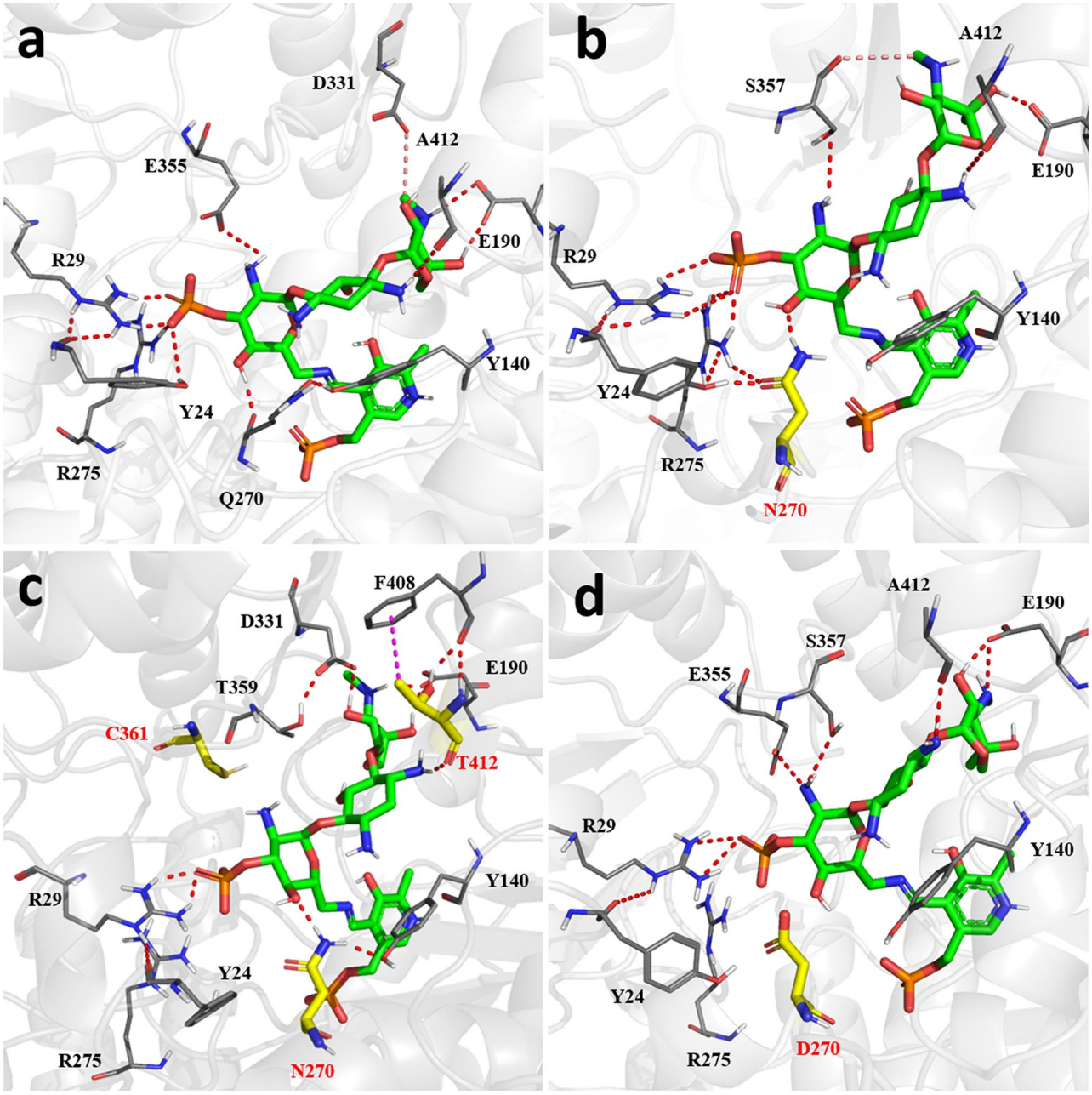

Fig. 6 Binding modes of GenB3^{WT} and its mutants with JI-20A-P. **a**. Interactions between GenB3^{WT} and JI-20A-P; **b**. Interactions between GenB3^{M1} and JI-20A-P; **c**. Interactions between GenB3^{M2} and JI-20A-P; **d**. Interactions between GenB3^{M3} and JI-20A-P. The green stick model represents JI-20A-P, the gray linear model indicates key residues in the binding pocket, the yellow stick model depicts the mutated amino acids, and the red dotted line represents hydrogen bonds

R29/R275. The distribution of conformations reveals that C361 does not directly interact with the substrate but instead forms indirect hydrogen bonds with the C2"-OH through T359 and D331. Additionally, T412 forms a hydrogen bond with the C1-NH_2, while the oxygen atom in the side chain of T412 establishes a new interaction with F408 (Fig. 6c). These interactions may contribute to the inward movement of the substrate in GenB3^{M2}.

To investigate the reasons behind the interactions of GenB3^{WT}, GenB3^{M1}, and GenB3^{M2} with JI-20Ba-P, MD simulations lasting 100 ns were conducted (Additional file 1: Fig. S12). Following stabilization, MM/GBSA calculations were employed to determine the binding free energies. The binding free energy for GenB3^{WT} was calculated to be -198.85 kcal/mol, whereas GenB3^{M2} exhibited a value of -226.24 kcal/mol (Table 4). This suggests that GenB3^{M2} demonstrates a more stable interaction

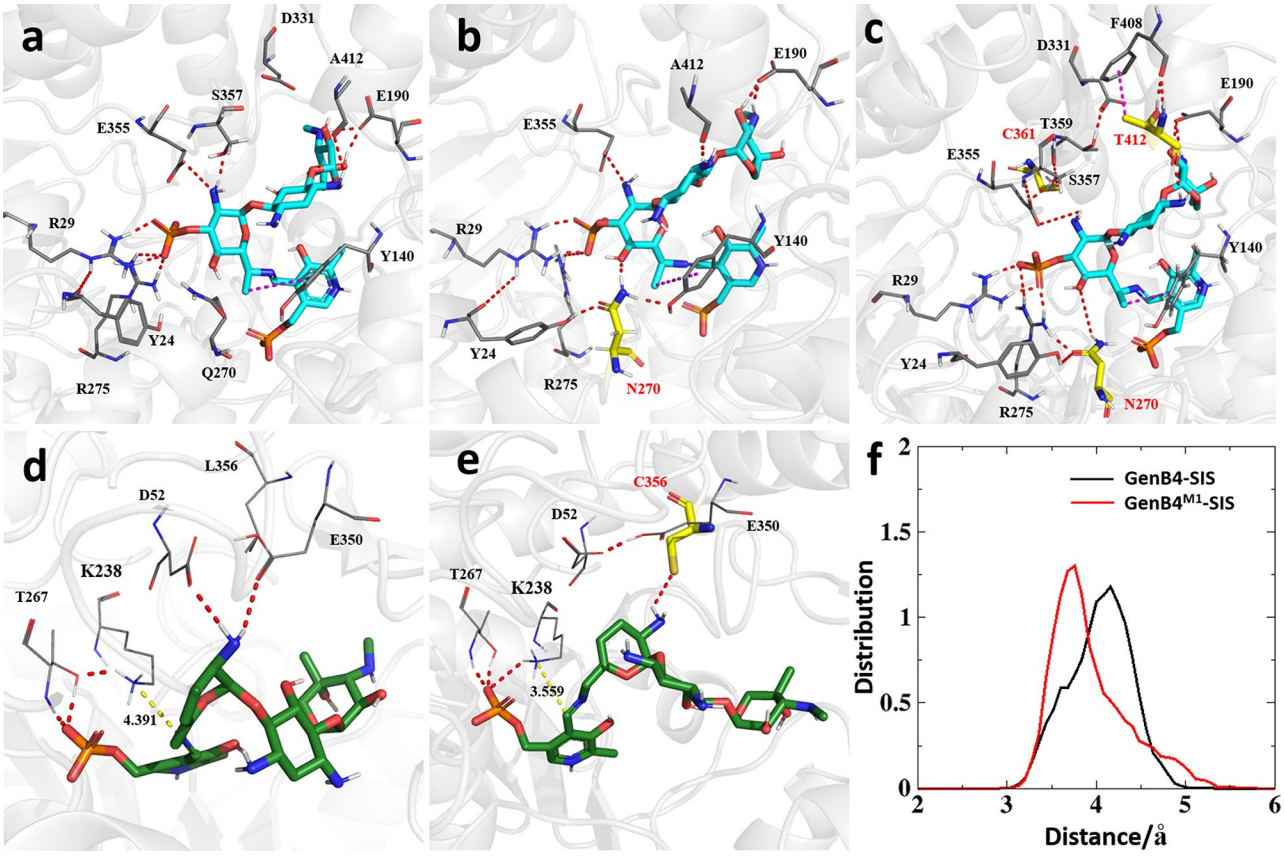

Fig. 7 Binding modes of mutants with JI-20Ba-P and sisomicin. **a**. Interactions between GenB3^{WT} and JI-20Ba-P; **b**. Interactions between GenB3^{M1} and JI-20Ba-P; **c**. Interactions between GenB3^{M2} and JI-20Ba-P; **d**. Interactions between GenB4^{WT} and sisomicin; **e**. Interactions between GenB4^{M1} and sisomicin; **f**. the catalytic distance distribution between GenB4^{WT} and GenB4^{M1}.The light blue stick model represents JI-20Ba-P, the dark green stick model represents sisomicin, the gray linear model indicates key residues in the binding pocket, the yellow stick model depicts the mutated amino acids, and the red dotted line represents hydrogen bonds

with JI-20Ba-P. Conformational analysis revealed that in GenB3^{WT}, the Q270 residue failed to form a hydrogen bond with the C4'-OH group (Fig. 7a), which contrasts with the binding mode observed in JI-20A-P, where the only distinction is the presence of an additional C6'-CH_3 group in JI-20Ba-P. In GenB3^{M1}, the shortened side chain of N270 appears to mitigate the steric hindrance imposed by the C6'-CH_3 group, not only restoring the hydrogen bond but also facilitating the formation of additional hydrogen bonds with Y24 and Y140 (Fig. 7b). The restoration of the hydrogen bond and the stabilization of catalytic residues contribute to the increased activity of GenB3^{M1}.

Upon superimposing GenB3^{WT} and GenB3^{M2}, it was found that JI-20Ba-P did not show significant movement (Additional file 1: Fig. S11b). Conformation analysis revealed that in GenB3^{M2}, the C6'-CH_3 interacted with Y140 through a σ-π interaction. This interaction was entirely present in GenB3^{WT}, GenB3^{M1}, and GenB3^{M2}. In GenB3^{M2}, C361 and T412 provide more interactions for JI-20Ba-P (Fig. 7c). Moreover, under the fixation effect of Y140, N270 continuously exerts a beneficial effect, which significantly enhances the catalytic activity of GenB3^{M2} towards JI-20Ba-P. Since JI-20A-P lacks the fixation effect of Y140, it is easily attracted by C361 and T412 and moves away from the catalytic residues, thus generating a negative effect among C361, T412, and N270. This may be the underlying reason why GenB3^{M2} shows an increased activity towards JI-20Ba-P but a decreased activity towards JI-20A-P.

Based on previous results, GenB4^{Q265N} reduced the catalytic activity of sisomicin. The activity was also reduced to varying degrees with the introduction of Q265N in the combination mutations (Table 3). However, in the reaction of GenB3 with JI-20A-P, GenB3^{Q270N} was beneficial to the reaction, which may be closely related to the change in the substrate. In the JI-20A-P, the C4'-OH interacts with N270, and the C3'-PO_3 interacts with Y24, R29, R275, and S57 through hydrogen bonds. These interactions do not exist in sisomicin, leading to a significant decrease in the substrate binding strength of GenB4, which is consistent with the MM/GBSA calculation results. The binding free energy of GenB4-sisomicin is -163.94 kcal/mol, while that of GenB3-JI-20A-P is

-223.39 kcal/mol (Table 4). Q265 cannot form hydrogen bonds with sisomicin, and thus the beneficial effect cannot be realized.

To investigate the reason for the L356C in GenB4, MD simulations of 100 ns were conducted for GenB4^{WT} and GenB4^{M1} with sisomicin (Additional file 1: Fig. S13). The MM/GBSA showed that the binding free energy of GenB4^{M1} with sisomicin was −171.31 kcal/mol. This indicates that GenB4^{M1} has better stability in binding to sisomicin compared to GenB4^{WT}. The conformation analysis showed that C356 forms a hydrogen bond with the C2'-NH_2 group, whereas the hydrogen bonds between D52 and E350 with the C2'-NH_2 group are absent (Fig. 7d, e). According to the catalytic mechanism, the reduction of the double bond in sisomicin is caused by the attack of K238 on the external aldimine formed from Sisomicin-PLP. Subsequently, the distance distribution between K238 and the external aldimine was analyzed. In GenB4^{WT}, this distance was 4.391 Å, while in GenB4^{M1}, it was 3.559 Å (Fig. 7f). This suggests that C356 indirectly shortens the distance between the active center and the catalytic residues, thereby accelerating the reaction process.

Conclusions

In this paper, sisomicin, Oxo-C1a, Oxo-Ver, and Oxo-C2a were synthesized enzymatically using GenB3 and GenB4, establishing a foundation for the chemoenzymatic synthesis of more AGs analogues. A semi-rational strategy was employed to enhance the activity of GenB3. The activity of GenB3^{M1} (Q270N) towards JI-20A-P was 1.74 times higher than that of GenB3^{WT}, while the activity of GenB3^{M2} (L361C/A412T/Q270N) towards JI-20Ba-P was 1.34 times higher than that of GenB3^{WT}. Through parallel amino acid, it was determined that the activity of GenB4^{M1} (L356C) towards sisomicin was 1.51 times higher than that of GenB4^{WT}, and the activity of GenB4^{M2} (L356C/A407T/Q265N) towards VerC2a was 1.34 times higher than that of GenB4^{WT}. Subsequently, engineering strains for sisomicin, Oxo-Ver, C1a, and Oxo-C2a were constructed, and the beneficial effects of the mutants were verified. MD simulations indicated that the primary reason for the enhanced activity of GenB3^{M1} was the formation of a hydrogen bond network. The increased activity of GenB4^{M1} was attributed to the reduced distance between K238 and the reactive center. The synergistic effect of L361C, A412T, and Q270N was observed only for JI-20Ba-P as the C6'-CH_3 provided additional stabilization, which was not the case for JI-20A-P. Our results not only establish a foundation for the synthesis of novel gentamicin analogues but also offer a reference for constructing a cell factory to synthesize more valuable single components of AGs in *M. echinospora*.

Methods

Microorganism and chemistry

M. echinospora and its knockout strains were used as hosts for the production of gentamicin and its intermediates, *Escherichia coli (E. coli)* Top10 serving as the cloning host, *E. coli* BL21(DE3) as the protein expression host, pET32a (+) as the expression vector for GenB3, and pET28a (+) as the expression vector for GenB4. The primers for the GenB3 and GenB4 mutants were synthesized by Nanjing GenScript Biotechnology Co., Ltd. *Pfu* polymerase was purchased from Sangon Biotech (Shanghai) Co. Ltd. and 2×GC Buffer, dNTPs, and T4 DNA ligase were obtained from Takara. The sequencing of the mutants was conducted by Suzhou GENEWIZ Biotechnology Co., Ltd. Growth medium (soluble starch 10 g/L, wheat bran 10 g/L, $MgSO_4{\cdot}7H_2O$ 5 g/L, $K_2HPO_4{\cdot}3H_2O$ 0.3 g/L, KNO_3 1 g/L, NaCl 0.5 g/L, $CaCO_3$ 1 g/L, asparagine 0.08 g/L, agar 2.5 g/L). Seed medium (soluble starch 15 g/L, soybean powder 1 g/L, glucose 1 g/L, KNO_3 0.5 g/L, $CaCO_3$ 23 g/L). Fermentation medium (soluble starch 50 g/L, soybean powder 35 g/L, glucose 15 g/L, corn powder 15 g/L, peptone 15 g/L, $(NH_4)_2SO_4$ 0.5 g/L, KNO_3 2.5 g/L, $CoCl_2{\cdot}6H_2O$ 0.01 g/L, $CaCO_3$ 26 g/L).

Separation and purification of phosphorylated substrates

The *M. echinospora* ΔKP, *M. echinospora* ΔB2P, and *M. echinospora* ΔP were selected to purify the intermediates JI-20A, JI-20Ba, and JI-20B. After acid treatment of the culture broth, the supernatant was applied onto 732× and 711× resins (Amicogen (China) Biopharm Co., Ltd), and bound substances were eluted with 2 mol/L $NH_3{\cdot}H_2O$. A second cation-exchange chromatography was performed on the weakly acidic resin, D152 (Amicogen (China) Biopharm Co., Ltd) and eluted with a gradient of $NH_3{\cdot}H_2O$ at varying concentrations (ranging from 0.01 to 0.30 mol/L). This process resulted in the yield of high concentrations of JI-20A, JI-20Ba, and JI-20B.

To obtain phosphorylated substrates, GenP was used to catalyze the intermediates obtained from the aforementioned separation. The reaction system consisted of substrates at a concentration of 4–8 mmol/L, Tris buffer (50 mmol/L, pH 7.0), ATP 10 mmol/L, $MgCl_2$ 10 mmol/L, and GenP 30 μmol/L, with the reaction conducted at 37 °C for 16 h. The reaction was ended in a boiled water bath and samples were centrifuged at 10,000 rpm for 10 min. The supernatant was then passed through a column of D152 and unbound compounds were discarded. The compound-bound column was washed with water followed by a gradient of $NH_3{\cdot}H_2O$ (ranging from 0.01 to 0.10 mol/L). Every fraction was checked by HPLC-ELSD. Then, the eluates of JI-20A-P, JI-20Ba-P, and JI-20B-P with higher purity were combined and concentrated.

HPLC-ELSD analysis of gentamicin C complexes and related intermediates

HPLC-ELSD analysis of mixtures was performed with a Welch C18 column (4.6 × 250 mm, 5 μm) connected to a SofTA Model 300s ELSD. The mobile phase I was a 92:8 mixture of 0.2 M TFA: methanol (0.8 ml/min), which was used in the GenP-catalyzed reaction, GenB3-catalyzed reaction, and the fermentation products. The mobile phase II was 0.2 M TFA (0.8 ml/ min), which was used in the reaction between GenB4 and sisomicin.

Molecular Docking

GenB3 (PDB ID: 7LM0) was prepared by removing all attached water molecules and adding hydrogen atoms. Multiple docking calculations were performed using Autodock 1.5.6 (https://autodock.scripps. edu) between JI-20A-P or JI-20A-P-PLP and GenB3. Each of the clustered conformations was analyzed individually. However, these conformations were deemed unreasonable for two reasons: First, the reaction center (C6'-NH_2) was too far from the position of PLP, making it impossible to form a covalent bond with PLP. Second, the conformations of JI-20A-P exhibited unreasonable distortions.

Given the amino acid sequences of GenB4 and GenB3 share 83.78% identity, and their crystal structures exhibit 0.47 Å RMSD, and considering that the PLP in both proteins is highly overlapping, we have reason to believe that the conformation of JI-20A-P-PLP in GenB3 is similar to that of C1a-PLP in GenB4. Due to the previously unsatisfactory docking results, we chose the C1a-PLP in GenB4 (PDB ID: 7LLD) as a starting point, added phosphate and hydroxyl groups, and then optimized the structure to obtain JI-20A-P-PLP. Since the binding sites of JI-20A-P-PLP and C1a-PLP are close, we overlapped GenB3 (PDB ID: 7LM0) and GenB4 (PDB ID: 7LLD), superimposed JI-20A-P-PLP and C1a-PLP, deleted the GenB4 and C1a-PLP, and obtained the initial binding conformation of GenB3 with JI-20A-P-PLP. Subsequently, we performed energy minimization to optimize the initial conformation, thereby reducing the adverse effects caused by the introduction of rigid groups. The binding models of GenB3 with JI-20Ba-P and JI-20B-P were obtained using the same method.

Site-directed mutagenesis

A detailed analysis of the binding pocket was conducted, selecting residues within a 5 Å range near the substrate as key amino acids. Homologous sequences to GenB3 were retrieved from UniProt and 16 sequences with homology greater than 35% were selected. These sequences were from the following species: *Zymobacter palmae* (A0A348HFA3), *Lonsdalea quercina* (A0A1H4EHM0), *Micromonospora inyonensis* (A0A1C6RDS9), *Actinokineospora iranica* (A0A1G6U9Y9), *Actinokineospora auranticolor* (A0A2S6GIE7), *Amycolatopsis cihanbeyliensis* (A0A542DRN1), *Actinoalloteichus hoggarensis* (A0A221VYX5), *Frankia casuarinae* (Q2J7L8), *Micromonospora olivasterospora* (Q2MG01), *Dactylosporangium matsuzakiense* (A0A9W6KGY7), *Streptomyces kanamyceticus* (Q6L741), *Streptomyces capitiformicae* (A0A919L608), *Micromonospora rosaria* (A0A136PS21), *Bradyrhizobium ivorense* (A0A508T828), *Streptomyces sp*. SID13726 (A0A6B2XAL9), *Streptomyces caeruleatus* (A0A101U365). We then aligned these sequences using MEGA11 and submitted the alignment results to WebLogo3 (https://weblogo.threeplusone.com) to obtain the sequence logo. Site-directed mutagenesis was achieved using overlapping extension PCR, and a similar method was applied to obtain combinatorial mutants.

Expression and purification of GenB3, GenB4 and its mutants

The BL21 (DE3) strain containing the mutant was grown in LB with Ampicillin to an OD_{600} of 0.6. Then, 0.1 mM IPTG was added, and the culture was induced at 16 °C for 20 h. After centrifugation, the cell pellet was collected. The pellet was washed and resuspended in 20 mL of Binding buffer, then sonicated for 20 min. After centrifugation for 20 min, the supernatant was loaded onto GE Healthcare's Ni Sepharose™ 6 Fast Flow. Approximately 30 mL of Binding Buffer was used to wash off the unbound proteins, followed by washing 30 mL of Buffer A (20 mmol/L Imidazole) and Buffer B (40 mmol/L Imidazole). The target protein was eluted using a 30 mL Elution Buffer (250 mmol/L Imidazole). The collection tubes containing the target protein were pooled together and dialyzed, and then 50% glycerol was added before storing at -80 °C.

Kinetic assay

The molybdenum blue method was used to detect the phosphate from the reaction to determine the initial reaction rates of each mutant. The enzyme reaction system was as follows: JI-20A-P and JI-20Ba-P were prepared at concentrations of 100–1900 μmol/L, α-ketoglutarate (α-KG) at 50 μmol/L, pyridoxal phosphate (PLP) at 0.75 mmol/L, and HEPES buffer at 50 mmol/L. The reaction mixture was preheated at 30 °C. Then, 10 μmol/L of GenB3 or the mutant was added. After a 15-minute reaction, 25 μL of the reaction solution was taken and added to a 96-well plate containing 75 μL of coloring solution. The reaction was allowed to proceed at room temperature for 5 min before adding 75 μL of stop solution. The absorbance was measured at 655 nm, and the amount of released phosphate and reaction rate were calculated using a standard curve made from K_2HPO_4 ($Y = 0.0005X + 0.0472$, $R^2 = 0.9994$) to determine the kinetic parameters of each mutant. The coloring solution

was prepared as follows: Solution A: 12% w/v L-ascorbic acid dissolved in 1 mol/L HCl; Solution B: 2% w/v ammonium molybdate tetrahydrate aqueous solution. Two parts of Solution A were mixed with one part of Solution B. The stop solution consisted of 2% sodium citrate and 2% acetic acid.

Construction of the engineered strains and verification of mutations in vivo

The knockout plasmid pD2925L was constructed to obtain *M. echinospora* ΔKL, *M. echinospora* B2L, and *M. echinospora* KB4L using a standard conjugation transfer method. To verify in vivo effects of beneficial mutants, plasmids pEAP4-*SRL*37-*gen*B3^{M1}, pEAP4-*SRL*37-*gen*B3^{M2}, pEAP4-*kas*Op*-*gen*B4^{M1} and pEAP4-*kas*Op*-*gen*B4^{M2} were constructed. Using the standard conjugation transfer method, GenB3^{WT} and GenB3^{M1} were introduced into *M. echinospora* ΔKB4L, GenB3^{WT}, and GenB3^{M2} into *M. echinospora* ΔB4, GenB4^{WT} and GenB4^{M1} into *M. echinospora* ΔKL, and GenB4^{WT} and GenB4^{M2} into *M. echinospora* ΔB2L. *M. echinospora* was grown in a growth medium at 34 °C to obtain spores. For the collection of products, *M. echinospora* was cultured in seed cultures at 34 °C for 48 h. Fermentation cultures were conducted for 120 h. Fermentation products of wild-type and mutant strains were adjusted to a pH of 2.0 with H_2SO_4. After centrifugation (5,000 rpm, 10 min), the supernatant was adjusted to a pH of 7.0 with NaOH. The fermentation broth was centrifuged again, and the supernatant was adsorbed by cationic resin D152. The products were washed with 0.2 M $NH_3{\cdot}H_2O$. The eluate was filtered through a 0.22 μm microporous membrane before subjection to HPLC-ELSD analysis.

Molecular dynamic simulation of the pre-reaction state

The AMBER20 molecular dynamics simulation software was utilized to conduct structural simulation and dynamic optimization of the enzyme-substrate complex system. For the protein part of the complex, the AMBER-ff14SB force field was employed, while for the small molecule compound part, the GAFF general force field was selected. Gaussian09 was used to optimize the structure of the small molecules and generate the bond angle parameters of the small molecules. The simulation system was constructed by immersing the entire system in a cubic box with periodic boundaries and filling the box with TIP3P water molecules, ensuring that the complex was at least 10 Å away from the edges of the box. Simultaneously, counterions were added to maintain the electroneutrality of the entire system. Firstly, energy minimization was carried out to eliminate the unnatural contacts within the entire system. Subsequently, with the solute part under harmonic potential restraint, the entire system was gradually heated from 0 K to 300.0 K and then equilibrated under the NPT ensemble at 300 K and 1 atm. Finally, a 100 ns production simulation was performed on the equilibrated system. To ensure the accuracy of the results, all systems were subjected to MD simulations three times under the same conditions and parameters. The CPPTRAJ program was used to analyze the simulation trajectories, and the root mean square deviation (RMSD), root mean square fluctuation (RMSF) of proteins and small molecules, as well as the radius of gyration during the simulation were calculated to analyze the structural changes of the systems. The MM/GBSA binding free energy calculation and energy decomposition of residues were carried out using the parallel version of the python script MMGBSA.py to evaluate the interaction relationship between the substrate and the enzyme and the key amino acid residues.

Supplementary Information

The online version contains supplementary material available at https://doi.org/10.1186/s12934-025-02678-0.

Supplementary Material 1

Acknowledgements

Not applicable.

Author contributions

HZ performed the experiments, analyzed the primary data, and prepared the manuscript. LY performed part of the in vitro experiments. QY analyzed the molecular mechanism of mutants by molecular dynamics simulations. ZK, JP, YJ, and BL assisted in product purification and mutants construction. XC and TT assisted in knockout experiments. XN supervised the experiments. HX and SZ supervised the whole research and revised the manuscript. All authors read and approved the final manuscript.

Funding

This work was supported by grants from the National Natural Science Foundation of China (81773613), the Natural Science Foundation of Liaoning (2023-MS-199), and the Scientific Research Fund of Liaoning Provincial Education Department (JYTZD2023135).

Data availability

No datasets were generated or analysed during the current study.

Declarations

Ethics approval and consent to participate

Not applicable.

Consent for publication

Not applicable.

Competing interests

The authors declare no competing interests.

Received: 17 December 2024 / Accepted: 18 February 2025
Published online: 27 February 2025

References

1. Schatz A, Bugie E, Waksman SA. Streptomycin, a substance exhibiting antibiotic activity against gram-positive and gram-negative bacteria. Clin Orthop Relat Res. 1944;2005:3–6.
2. Saravolatz LD, Stein GE. Plazomicin: A new aminoglycoside. Clin Infect Dis. 2020;70:704–9.
3. Bidou L, Bugaud O, Belakhov V, Baasov T, Namy O. Characterization of new-generation aminoglycoside promoting premature termination codon readthrough in cancer cells. RNA Biol. 2017;14:378–88.
4. Izadi Z, Barzegari E, Iranpanah A, Sajadimajd S, Derakhshankhah H. Gentamycin rationally repositioned to inhibit miR-34a ameliorates oxidative injury to PC12 cells. ACS OMEGA. 2023;8:771–81.
5. Childs-Disney JL, Yildirim I, Park H, Lohman JR, Guan L, Tran T, Sarkar P, Schatz GC, Disney MD. Structure of the myotonic dystrophy type 2 RNA and designed small molecules that reduce toxicity. ACS Chem Biol. 2014;9:538–50.
6. Rzuczek SG, Park H, Disney MD. A toxic RNA catalyzes the in cellulo synthesis of its own inhibitor. Angew Chem Int Ed. 2014;53:10956–9.
7. Wang M, Wu B, Shah SN, Lu P, Lu Q. Aminoglycoside enhances the delivery of antisense morpholino oligonucleotides in vitro and in Mdx mice. Mol Therapy - Nucleic Acids. 2019;16:663–74.
8. Rajasekaran P, Crich D. Synthesis of gentamicin minor components: gentamicin B1 and gentamicin X2. Org Lett. 2020;22:3850–4.
9. Hanessian S, Szychowski J, Maianti JP. Synthesis and comparative antibacterial activity of verdamicin C2 and C2a. A new oxidation of primary allylic Azides in dihydro[2H]pyrans. Org Lett. 2009;11:429–32.
10. Jana S, Crich D. Synthesis of gentamicin minor components: gentamicin C1a and gentamicin C2b. Org Lett. 2022;24:8564–7.
11. Jana S, Rajasekaran P, Haldimann K, Vasella A, Böttger EC, Hobbie SN, Crich D. Synthesis of gentamicins C1, C2, and C2a and antiribosomal and antibacterial activity of gentamicins B1, C1, C1a, C2, C2a, C2b, and X2. ACS Infect Dis. 2023;9:1622–33.
12. Xu J, Zhang X, Xu G, Zhang Y, Li H, Shi J. Design, synthesis and activity evaluation against Drug-Resistant Bacteria of 6′-Amidine modified aminoglycoside derivatives. ChemistrySelect. 2024;9:e202303210.
13. Ban YH, Song MC, Jeong JH, Kwun MS, Kim CR, Ryu HS, Kim E, Park JW, Lee DG, Yoon YJ. Microbial enzymatic synthesis of Amikacin analogs with antibacterial activity against Multidrug-Resistant pathogens. Front Microbiol. 2021;12:725916.
14. Lee NJ, Kang W, Kwon Y, Oh JW, Jung H, Seo M, Seol Y, Wi JB, Ban YH, Yoon YJ, Park JW. Chemo-enzymatic synthesis of Pseudo-trisaccharide aminoglycoside antibiotics with enhanced nonsense Read-through inducer activity. ChemMedChem. 2023;18:e202200497.
15. Stojanovski G, Hailes HC, Ward JM. Facile and selective N-alkylation of gentamicin antibiotics via chemoenzymatic synthesis. Green Chem. 2022;24:9542–51.
16. Chen X, Zhang H, Zhou S, Bi M, Qi S, Gao H, Ni X, Xia H. The bifunctional enzyme, GenB4, catalyzes the last step of gentamicin 3′,4′-di-deoxygenation via reduction and transamination activities. Microb Cell Fact. 2020;19:62.
17. Li SC, Bury PD, Huang FL, Guo JH, Sun G, Reva A, Huang C, Jian XY, Li Y, Zhou JH, et al. Mechanistic insights into dideoxygenation in gentamicin biosynthesis. ACS Catal. 2021;11:12274–83.
18. Zhou S, Chen X, Ni X, Liu Y, Zhang H, Dong M, Xia H. Pyridoxal-5′-phosphate-dependent enzyme GenB3 catalyzes C-3′,4′-dideoxygenation in gentamicin biosynthesis. Microb Cell Fact. 2021;20:65.
19. Kong Z, Tian T, Wang R, Xia H, Sun J, Zhai H, Ni X. Enhanced activity of C-3′ and C-4′ dideoxygenation of the aminoglycoside GenB3 by a semi-rational design strategy. Mol Catal. 2024;565:114380.
20. Gawronski JD, Benson DR. Microtiter assay for glutamine synthetase biosynthetic activity using inorganic phosphate detection. Anal Biochem. 2004;327:114–8.
21. Gu Y, Ni X, Ren J, Gao H, Wang D, Xia H. Biosynthesis of epimers C2 and C2a in the gentamicin C complex. ChemBioChem. 2015;16:1933–42.

Publisher's note